

A Smoothed Particle Hydrodynamics Approach for Efficient 3D Process Modeling of Linear Friction Welding

Quang Truong¹ and Srujan Rokkam^{2,3}
Advanced Cooling Technologies, Inc., Lancaster PA 17601, USA

Michael Eff⁴
Edison Welding Institute, Columbus OH 43221, USA

Linear friction welding (LFW) is a solid-state joining process in which a weld between two metals is formed by combined action of heating via plastic deformation and forming force that creates a weld interface. The technique is increasingly attracting attention in aerospace industry, due its several advantages like absence of solidification defects, no requirement for external heat source, and the mechanical and fatigue properties of the weld being equivalent or surpassing the parent material. Due to large deformation, commercially available software tools are limited to modeling of LFW in 2D using Finite Element Method (FEM) with adaptive mesh controls. In this work, we developed a meshless approach that utilizes Smoothed Particle Hydrodynamics (SPH) to obtain a physics-based model capable of capturing the thermo-mechanical behavior LFW process in 3D. The meshless framework is implemented using a commercial finite element analysis package using custom defined application programming interface. Subsequently, we employed the developed model to simulate and investigate flash formation and burn-off distance of LFW of Ti-6Al-4V workpieces. The SPH simulation results agreed well with FE simulation and experimental data. The model demonstrated computational efficiency of approximately 16 hours to simulate 3 seconds of LFW process with a 12-core desktop workstation. This work was undertaken under a SBIR Phase II program funded by The U.S. Air Force, Contract FA8650-19-C-5050, awarded to ACT, Inc.

I. Nomenclature

<i>LFW</i>	=	linear friction welding
<i>SFW</i>	=	friction stir welding
<i>FEM</i>	=	finite element method
<i>SPH</i>	=	smoothed particle hydrodynamics
<i>ALE</i>	=	arbitrary lagrangian-eulerian
<i>HAZ</i>	=	heat affected zone
<i>TMAZ</i>	=	thermo-mechanically affected zone
<i>PZ</i>	=	plastic zone
$W(R, h)$	=	smoothing kernel function, as a function of distance between particles R and smoothing length h
α, β	=	space indices
m, m_i	=	mass, mass of particle i
v, v_i^β	=	velocity, velocity of particle i component in β direction

¹ Engineer II, Research & Development.

² Engineering Manager, Research & Development.

³ *Corresponding author* email: srujan.rokkam@1-act.com .

⁴ Senior Engineer.

ρ, ρ_i = density, density of particle i
 σ = Cauchy stress
 k = thermal conductivity
 E_T = energy
 μ = coefficient of friction

Indicial notation applies in descriptions of vectors, tensors and differential equations.

II. Introduction

Linear friction welding (LFW) is one of the three variants of solid-state friction welding: rotary, linear, and orbital^{1,2,3,4}. In LFW, the heat is generated via oscillating linear movement of one component relative to the other to soften the interface material, as shown in Fig. 1. LFW offers numerous advantages including: efficient conversion of mechanical into thermal energy, absence of melting and re-solidification processes, small heat affected zone (HAZ), as well as suitability for joining difficult-to-weld, high performance, and dissimilar materials. However, LFW also has several disadvantages, such as formation of flash and requirement of complex and precise control systems⁵.

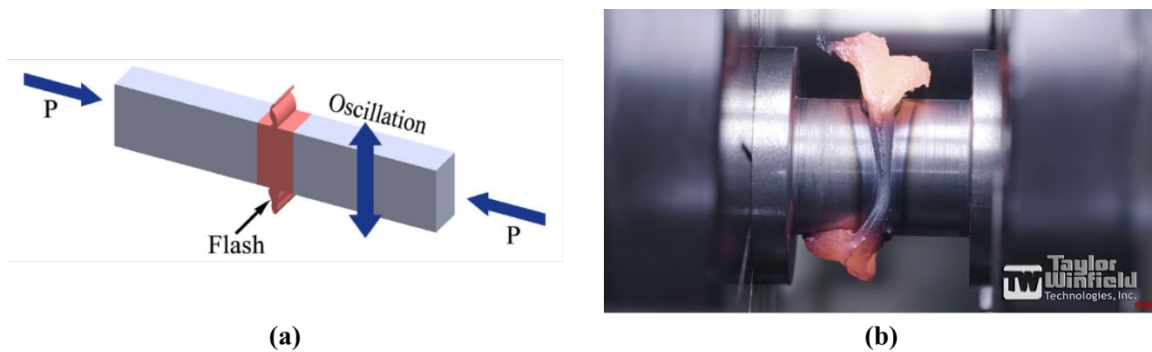


Fig. 1 (a) Schematic of Linear Friction Welding Process⁴, (b) Actual Welding Process⁶.

Current commercially available finite element software (FORGE, DEFORM, ANSYS, and ABAQUS) are limited to modeling linear friction welding in two dimensions with the Arbitrary Lagrangian-Eulerian (ALE) adaptive mesh control^{4,7}. The ALE adaptive mesh control is used to effectively overcome the excessive finite element distortion during LFW process. The ALE approach first solves a Lagrangian time-step, then performs a Eulerian/advection step to remap the distorted Lagrangian mesh and material solutions onto a spatially fixed Eulerian mesh. The use of 2D analysis to simulate a complex 3D process like LFW is a considerable limitation⁸. Li et al⁷ demonstrated the need for 3D modeling to get better accuracy in capturing heat generated by friction, axial shortening, residual stresses, and flash/ridges formation (and 2D models are limited in capturing them). However, FEM with adaptive re-meshing in 3D is extremely computationally expensive and requires special numerical algorithms. In addition, the element deformation in the weld zone is much larger in 3D than in 2D, an aspect which is likely to cause numerical errors in re-meshing stage.

The research work of this paper presents the development of a Smoothed Particle Hydrodynamics (SPH) based approach for modeling of linear friction welding process. The SPH method is a meshless Lagrangian approach capable of solving computational fluid dynamics and continuum solid mechanics problems with large deformations⁹. Recently, a number of research groups have worked on simulating friction stir welding process (FSW) using SPH method^{10,11,12}.

III. Modeling of Linear Friction Welding Process

A. Implementation of LFW Model into LS-DYNA

The SPH method utilizes smoothing kernel function W , where physical properties of a particle are accounted for by other particles within its neighborhood. The mesh-free nature of SPH makes it ideally suited for numerical simulation of the LFW process. The SPH formulation of the continuum governing equations are modified based on the damage mechanics equations to include the smoothing function $W(R, h)$, where:

Conservation of mass becomes:

$$\frac{d\rho_i}{dt} = \rho_i \sum_{j=1}^{N_i} \frac{m_j}{\rho_j} (v_i^\beta - v_j^\beta) \frac{\partial \mathbf{W}_{ij}}{\partial x_i^\beta} \quad (1)$$

Conservation of momentum becomes:

$$\frac{dv_i^\alpha}{dt} = - \sum_{j=1}^{N_i} m_j \left(\frac{\sigma_i^{\alpha\beta}}{\rho_i^2} + \frac{\sigma_j^{\alpha\beta}}{\rho_j^2} \right) \frac{\partial \mathbf{W}_{ij}}{\partial x_i^\beta} \quad (2)$$

Conservation of energy becomes:

$$\frac{dE_T}{dt} = \sum_j \frac{m_j}{\rho_i \rho_j} \frac{k_i - k_j}{|x_{ij}|^2} x_{ij} \nabla_i \mathbf{W}_{ij} \quad (3)$$

The frictional heat generation is needed for modeling of LFW process. Frictional heat generation can be calculated using Coulomb friction law as well as flow stress. Coulomb friction law is only applied at early stage of welding when interface temperature is low. As the interface material is plasticized, heat generation is dependent on plastic deformation because the friction behavior is dominated by viscoplastic friction⁴.

$$Q = \max(\text{Coulomb friction}, \text{flow stress}) = \max(\mu \cdot Fx \cdot Vy, \sigma) \quad (4)$$

In LS-DYNA, the temperature boundary condition can be applied as boundary condition with a curve function, as shown below, with n is the element ID.

$$\text{MIN} \left(\text{MAX}(T0, \text{TEMP}(n)) + \text{ABS}(FX(n)) * \text{fric_co} * \text{ABS}(VY(n)), \text{ELHIST}(n, 0, 9, -1, 0) \right) \quad (5)$$

In this work, the SPH model for LFW was developed in LS-DYNA simulation software package, where frictional heat generation and material properties were implemented as user defined functions. 3D simulations of LFW process with two distinct workpieces were performed, as shown in Fig. 2. The left workpiece was under pressure in horizontal direction (x-direction), and the right workpiece was under oscillation motion in vertical direction (y-direction). Each workpiece has a rectangular section of $90 \times 20 \times 15$ mm, and a neck section of $75 \times 5 \times 10$ mm. The material properties of the workpieces are based on Ti-6Al-4V properties. Table 1 shows the frequency, amplitude, and welding pressure.

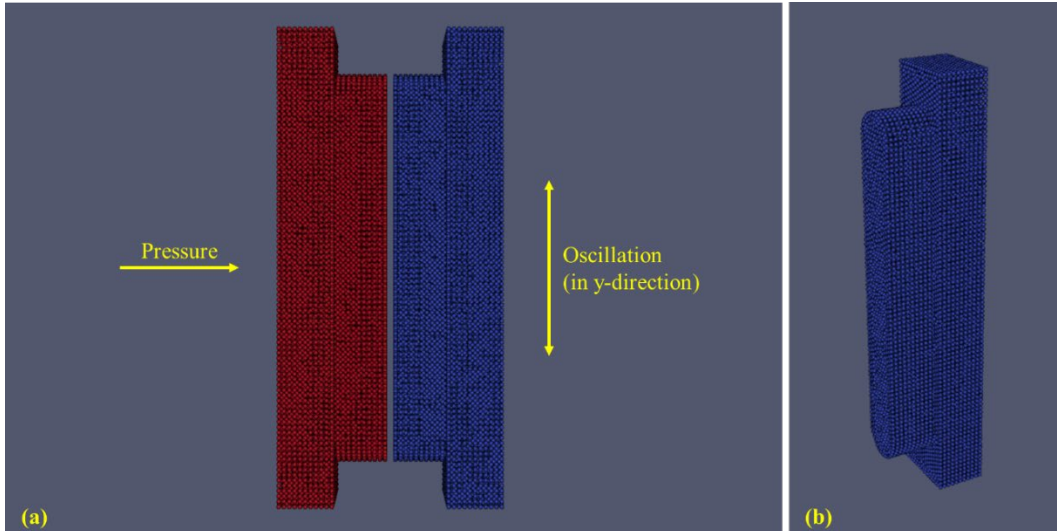


Fig. 2 Simulation of LFW process with two distinct Ti-6Al-4V workpieces: (a) the left workpiece (colored in red) was under pressure in x-direction, the right workpiece (colored in blue) was under oscillation in y-direction, (b) isometric view of the right workpiece, the rectangular section is $90 \times 20 \times 15$ mm and the neck section is $75 \times 5 \times 10$ mm.

Table 1 Operating conditions for 3D simulation of LFW process of 2 SPH workpieces.

Frequency (Hz)	40
True Amplitude (mm)	1.5
Weld Pressure (Pa)	1.034e8

Fig. 3 and Fig. 4 show the temperature profile of the workpieces during LFW process up to 2 seconds. At 1 second, the temperature at the weld interface raised to 1500 K due to frictional heat, and flash formation started to occur. The conduction of the heat generated at the Plastic Zone (PZ) leads to the increase in temperature in TMAZ and HAZ of the weld pieces. During the LFW process, the oscillatory motion of the workpieces pushes the thermally softened material out of the junction to form the flash. The welding phase was stopped at 2 seconds. At this time, the flash formation had the expected pattern, where the plasticized material was extruded in both oscillating directions (y-direction) and non-oscillating direction (z-direction).

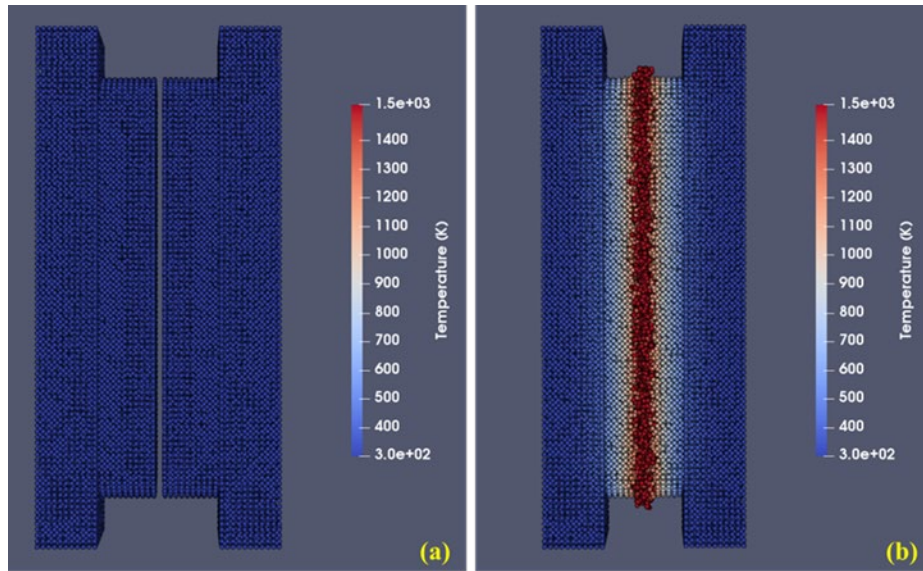


Fig. 3 Temperature profile of two Ti-6Al-4V workpieces during LFW process: (a) At time $t = 0.0$ s, (b) At time $t = 1.0$ s

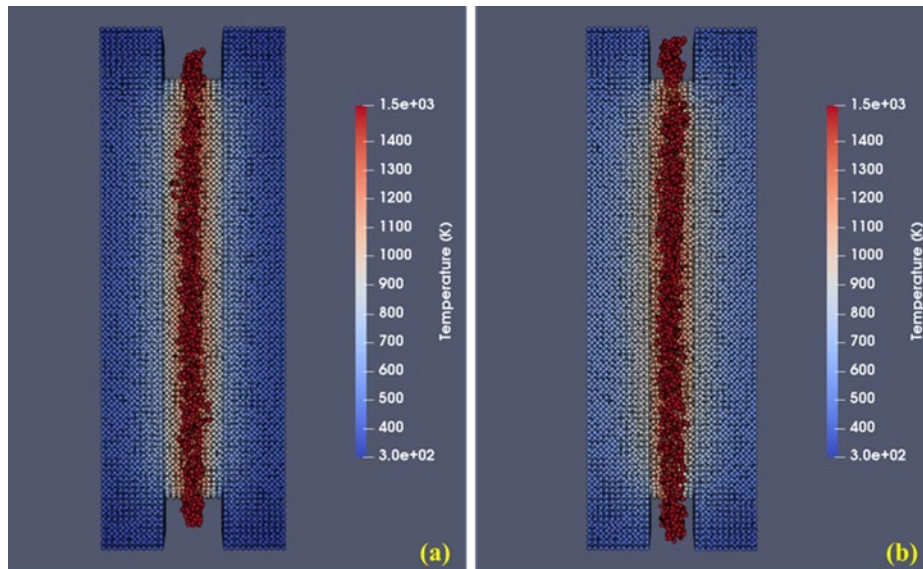


Fig. 4 Temperature profile of two Ti-6Al-4V workpieces during LFW process: (a) At time $t = 1.5$ s, (b) At time $t = 2.0$ s

To validate the SPH model results, experimental welding trials of Ti-6Al-4V workpieces were performed. The upset and weld time of experimental welding trials were to be used to validate the model.

B. Sensitivity Study on Influence of Material Properties on Flash Formation

A sensitivity study on influence of material properties on LFW flash formation was performed. The material properties of Ti-6Al-4V for two selected cases are shown in Table 2 and Table 7. The properties vary with increasing temperature from 200 K to 3000 K. The properties at 200 K and 3000 K are also lower and upper bounds to avoid numerical errors, such as when local temperatures in the workpiece go to slightly below room temperature (299.9 K).

Case 1:

Table 2 Material properties of Ti-6Al-4V at different temperatures for case 1 study. The properties at 200K and 3000K are lower and upper boundary reference only.

Temperature (K)	200	300	1050	1100	1150	1200	1300	3000
Young's modulus (kPa)	1.138 e8	1.138 e8	8.270 e7	7.240 e7	6.210 e7	5.520 e7	5.000 e7	1.000 e7
Prandtl's number	0.342	0.342	0.342	0.342	0.342	0.342	0.342	0.342
Coefficients of thermal expansion (K ⁻¹)	7.808 e-6	8.98 e-6	9.03 e-6	9.191 e-6	8.930 e-6	8.39 e-6	8.398 e-6	8.398 e-6
Yield stress (kPa)	1.138 e7	1.138 e7	8.270 e5	7.240 e5	6.210 e5	5.520 e5	1.000 e5	1.000 e4
Tangent modulus	0.1	0.1	0.1	0.1	0.1	0.1	0.1	0.1

Fig. 5 and Fig. 6 show the LFW process to 2 seconds. At 1 second, the temperature at the weld interface raised to 1500 K due to frictional heat, and flash formation started to occur. Again, the conduction of the heat generated at the Plastic Zone (PZ) leads to the increase in temperature in TMAZ and HAZ of the weld piece. During the LFW process, the oscillatory motion of the workpieces pushes the thermally softened material out of the junction to form the flash. At 2 seconds, the flash formation had the expected pattern.

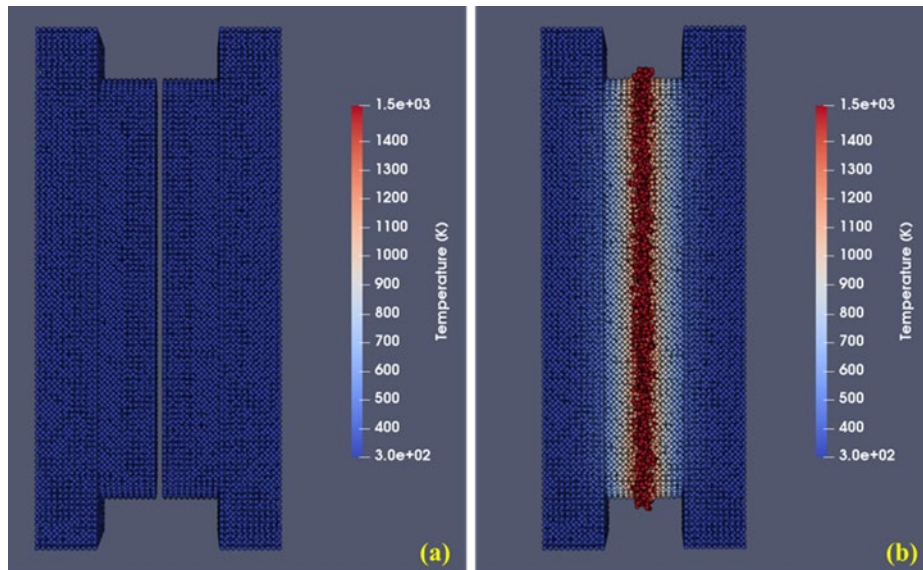


Fig. 5 Temperature profile of two Ti-6Al-4V workpieces during LFW process, using material properties in Table 2: (a) time $t = 0.0$ s, (b) time $t = 1.0$ s.

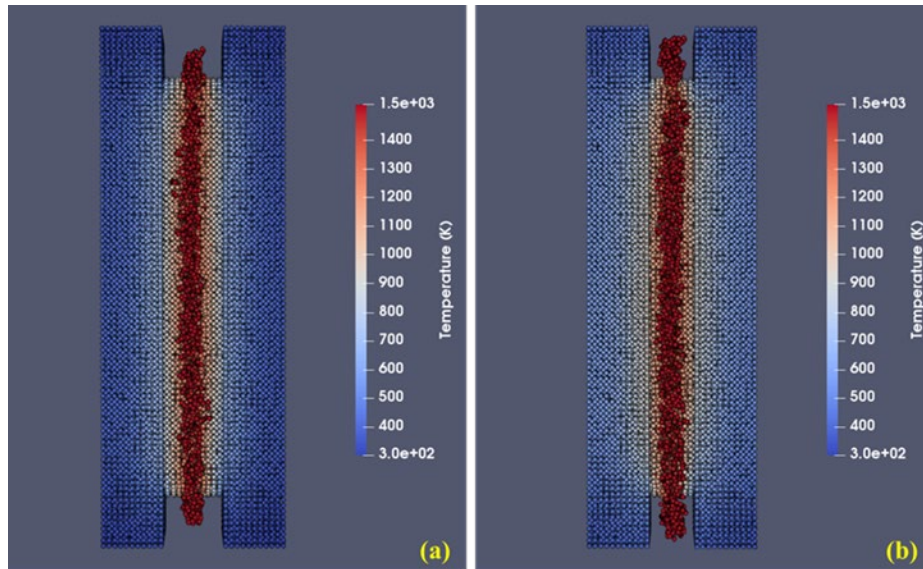


Fig. 6 Temperature profile of two Ti-6Al-4V workpieces during LFW process, using material properties in Table 2: (a) time $t = 1.5$ s, (b) time $t = 2.0$ s.

Case 2:

Table 3 Material properties of Ti-6Al-4V at different temperatures for case 2 study. The properties at 200K and 3000K are lower and upper boundary reference only. The differences compared to case 1 are in gray.

Temperature (K)	200	300	1050	1100	1150	1200	1300	3000
Young's modulus (kPa)	1.138 e8	1.138 e8	8.270 e7	7.240 e7	6.210 e7	5.52 0 e7	1.000 e7	5.000 e6
Prandtl's number	0.342	0.342	0.342	0.342	0.342	0.342	0.342	0.342
Coefficients of thermal expansion (K ⁻¹)	7.808 e-6	8.98 e-6	9.03 e-6	9.191 e-6	8.930 e-6	8.39 e-6	8.398 e-6	8.398 e-6
Yield stress (kPa)	1.138 e7	1.138 e7	8.270 e5	7.240 e5	6.210 e5	5.520 e5	5.000 e4	1.000 e4
Tangent modulus	0.1	0.1	0.1	0.1	0.1	0.1	0.1	0.1

Fig. 7 and Fig. 8 show the LFW process to 1.75 seconds. In this case #2, the Young's modulus and yield stress at 1300 K were smaller than case #1. Thus, we expected the flash of this case #2 to be thinner and weaker than case #1. During the LFW process, the frictional heat raised the temperature at the interface, similar to previous cases. The flash formation occurred at 1.0 second, but the flash was thinner as expected. At 1.75 second, a small outer part of the flash got disconnected and fell off the weld.

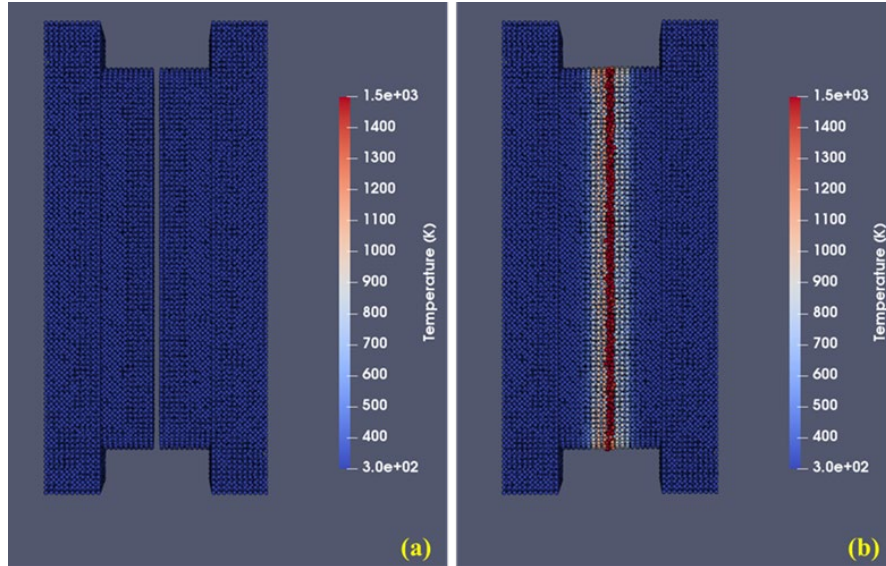


Fig. 7 Temperature profile of two Ti-6Al-4V workpieces during LFW process, using material properties in Table 3: (a) time $t = 0.0$ s, (b) time $t = 0.25$ s.

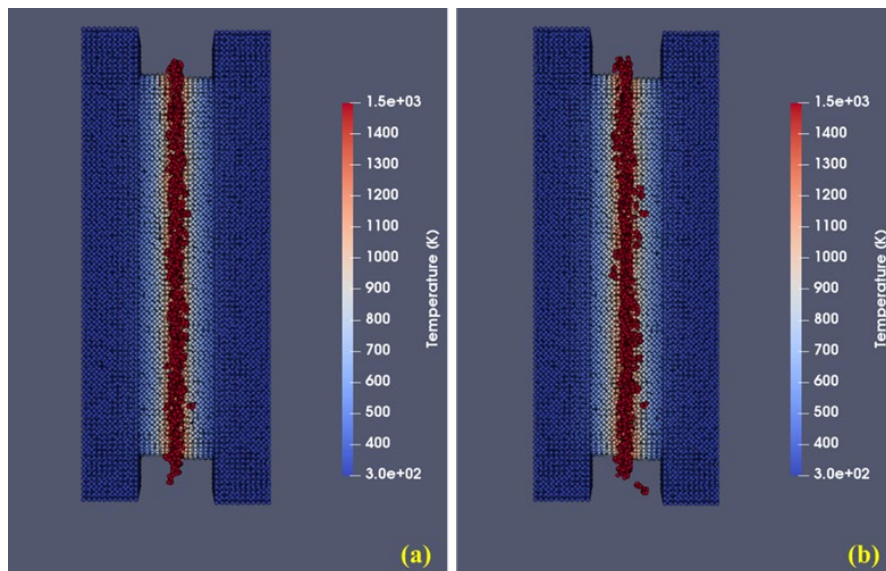


Fig. 8 Temperature profile of two Ti-6Al-4V workpieces during LFW process, using material properties in Table 3: (a) time $t = 0.0$ s, (b) time $t = 0.25$ s. At 1.75s, a small part of the flash was disconnected.

C. Sensitivity Study on Influence of Force Versus Heat Generation on Flash Formation

The heat generation is a function of the force applied and particle's velocity, as well as flow stress when material is plasticized. The force applied to each particle on the left workpiece is 14 N/particle, corresponding to $1.034e8$ Pa of pressure applied, shown in Table 1. The material properties of the workpieces are from Table 2. In Fig. 9, the force of 14 N was applied to each particle in the first three left layers of the left workpiece. Under this condition, the left workpiece experienced some buckling/cracking phenomenon before softening. The temperature due to friction increased to only 600K, which would not soften the Ti-6Al-4V material significantly. Therefore, the buckling/cracking must come from either excessive force or programmatic error in LS-DYNA. The cracking of the left workpiece occurred when the stress value went above 5 MPa. If the force applied can be reduced to maintain the effective stress below 5MPa, cracking would not occur.

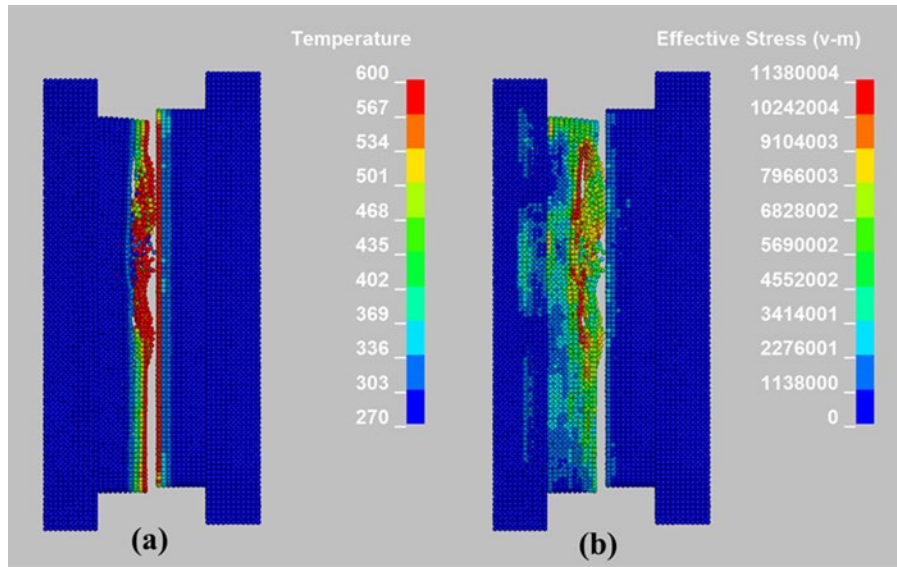


Fig. 9 3D simulation of LFW of Ti-6Al-4V material from Table 2: (a) Temperature profile, (b) Effective stress profile. The force applied is 14 N/particle. The left workpiece experienced cracking and deformation before softening. Thus, the 14N/particle force applied was too high.

Fig. 10 shows a simulation of LFW with material in Table 2, with the force reduced to 1.4 N/particle. Consequently, the value of penalty factor $pfact$ must be reduced from 1.0e5 to 1.0e3 to avoid excessive particle's bouncing-back. In this case, the temperature raised not only the 1st layer but evenly throughout the entire interface boundary, which is not correct. In addition, the temperature also incorrectly raised higher at the top and bottom corner on the right workpiece, compared to the rest of the workpiece. The reason for the increase in temperature in the entire interface boundary is that 1.4 N/particle is too low. The force in the x -direction (horizontal direction) is small compared to the force magnitude. The force in the x -direction being too small would also explain the higher temperature at the top and bottom corner on the right workpiece, since the force in y -direction of the right workpiece is surely higher than x -direction.

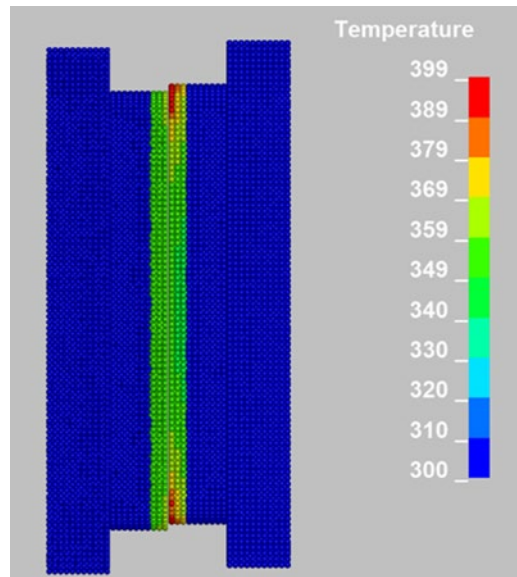


Fig. 10 3D simulation of LFW of Ti-6Al-4V material from Table 2. The force applied is 1.4 N/particle. The temperature profile is shown. Temperature raised not only the 1st layer but evenly throughout the entire interface boundary, which is not correct.

Multiple simulations with the operating conditions in Table 1 were run to investigate the sensitivity of the model response to penalty factor (PFACT) for SPH particle contact. In LS-DYNA, SPH particles from different parts can

contact via *DEFINE_SPH_TO_SPH_COUPLING with a penalty scale factor, PFACT. PFACT influences the spring constant of contact algorithm. Small value of less than 1 is recommended for low velocity contact between two SPH parts, while high value of more than 10 is suitable for stiff interaction ¹³. Since the SPH modeling framework of LS-Dyna is not developed with LFW modeling in mind, there is a need to understand the sensitivity of the penalty factor to modeling LFW appropriately. Based on the sensitivity analysis of the model to PFACT, we identified that a PFACT value of 10^5 (or $1.0e5$) to be suitable for LFW conditions. Consequently, the force boundary condition can be applied instead of displacement.

IV. Experimental Verification and Validation of LFW model

D. Scaling Trials

All welding trials occurred on Edison Welding Institute’s 20-ton Taylor Winfield linear friction welding machine. Each weld was subject to metallographic analysis, tensile testing, and monitored for process responses. The welds were run in burn-off control to protect the equipment from over-upsetting and crashing into itself. As a result, the duration of the weld stage was variable and was mapped a response. Since the model is run in the same duration, it is crucial to map the relationship between upset and weld duration. The welding trials were conducted in two manners. The goal was to conduct a design of experiments (DOE) to map the process space to metallurgical weld quality, tensile strength, and process responses such as shear load, upset, and flash profile. To prepare for the DOE, scaling trials are needed to set the bounds of the investigation. Seven scaling trials were conducted, and the parametric inputs are summarized in Table 4. Several variables were held constant, Stick-out was 12.5 mm based on the sample geometry. A low-pressure scrub stage occurred for each weld at 23 MPa for 0.2 s before the weld stage at the prescribed frequency and amplitude for a given weld. Each weld also maintained the weld pressure for 5 s after cessation of oscillation. Each weld was controlled in burn-off control, meaning oscillation continued until the prescribed loss of length is achieved. In this mode the weld stage time is variable. Each condition resulted in a visually acceptable weld.

Table 4 Scaling trials parameter matrix.

Weld ID	Oscillator	Fixed	Frequency	Amplitude	Weld Pressure	Program Burn-off
	Material	Material	Hz	mm	MPa	mm
64-1	Ti-6Al-4V	Ti-6Al-4V	35	2.5	100	3.5
64-2	Ti-6Al-4V	Ti-6Al-4V	20	3	62	2.5
64-3	Ti-6Al-4V	Ti-6Al-4V	60	1.5	100	2
6242-1	Ti-6Al-2Sn-4Zr-2Mo	Ti-6Al-2Sn-4Zr-2Mo	35	2.5	100	3.5
6242-2	Ti-6Al-2Sn-4Zr-2Mo	Ti-6Al-2Sn-4Zr-2Mo	50	2	140	2.5
Dis-1	Ti-6Al-4V	Ti-6Al-2Sn-4Zr-2Mo	35	2.5	100	3.5
Dis-2	Ti-6Al-4V	Ti-6Al-2Sn-4Zr-2Mo	50	2	140	2.5

E. Statistics Based Experimental Design

The scaling trials laid the groundwork for the design of experiments. A resolution IV fractional DOE was selected for this work. The inputs or variables that were investigated included material combination, peak surface velocity (function of amplitude and frequency), weld pressure and weld burn-off (loss of length). The outputs measured included: tensile strength, upset length, shear forces, upset rate, and weld quality. The raw DOE design is displayed in Table 5, and is shown for 5 two-level variables, which are required for this experiment.

Table 5 Resolution IV 12-run raw DOE design.

Trial	Factor				
	A	B	C	D	E
1	1	1	1	-1	-1
2	1	1	1	1	1
3	-1	-1	-1	1	1
4	-1	-1	-1	-1	-1
5	1	-1	1	1	1
6	-1	1	-1	1	1
7	1	-1	1	-1	-1
8	-1	1	-1	-1	-1
9	1	-1	-1	-1	1
10	-1	1	1	1	-1
11	-1	1	1	-1	1
12	1	-1	-1	1	-1

The resolution IV design shows all single-factor interactions directly, but some two-factor confound. Confounding is the event where two interaction such A*E and C*E are statistically indistinguishable due to the design. This occurs in this study due to sacrifice in resolution to get the number of trials down (12 vs. 32 for full resolution). The confounding scheme is displayed in Table 6. The confounding scheme led to variable interactions and which pairs were confounded based on prior expertise.

Table 6 Confounding two-level variable layout.

Two Factor Interaction	Confounding Pair
-AB	unconfounded
-BC	unconfounded
AE	-CD
-DE	-AC
-BD	unconfounded
-BE	unconfounded
-CE	-AD

For this experiment, Columns A and B were combined to create a three-level variable to represent the three material joining combinations used in the DOE, Ti-6Al-4V to Ti-6Al-4V, Ti-6Al-2Sn-4Zr-2Mo to Ti-6Al-2Sn-4Zr-2Mo and Ti-6Al-4V to Ti-6Al-2Sn-4Zr-2Mo. The material combinations must not confound. Thus, the selection of columns A and B for the three-level variable or the effects of the material combinations would not be determinable. Pressure was assigned to column C, Surface velocity to column D and Burn-Off to column E. The levels were set to two levels for each of these variables, a high and low value. The resultant experiment design is displayed in Table 7.

Table 7 Experimental matrix for DOE trials with input variables.

Trial	Factor			
	Material(s)	Pressure (MPa)	Surface Velocity (mm/s)	Burn-Off (mm)
1	Ti-6Al-4V to Ti-6Al-4V	140	Low	Low
2	Ti-6Al-4V to Ti-6Al-4V	140	High	High
3	Ti-6242 to Ti-6Al-2Sn-4Zr-2Mo	100	High	High

4	Ti-6242 to Ti-6Al-2Sn-4Zr-2Mo	100	Low	Low
5	Ti-6Al-4V to Ti-6Al-2Sn-4Zr-2Mo	140	High	High
6	Ti-6Al-4V to Ti-6Al-2Sn-4Zr-2Mo	100	High	High
7	Ti-6Al-4V to Ti-6Al-2Sn-4Zr-2Mo	140	Low	Low
8	Ti-6Al-4V to Ti-6Al-2Sn-4Zr-2Mo	100	Low	Low
9	Ti-6Al-4V to Ti-6Al-2Sn-4Zr-2Mo	100	Low	High
10	Ti-6Al-4V to Ti-6Al-2Sn-4Zr-2Mo	140	High	Low
11	Ti-6Al-4V to Ti-6Al-2Sn-4Zr-2Mo	140	Low	High
12	Ti-6Al-4V to Ti-6Al-2Sn-4Zr-2Mo	100	High	Low

F. Experimental Results

Twelve welds were performed, and each weld was subject to metallographic analysis, tensile testing, and monitored for process responses. A summary of the outputs related to the process and mechanical testing are displayed in Table 8. The weld durations vary from 0.7-s up to 2.7-s, and upset varied from 2.39-mm up to 5.18-mm. These variations show a wide range of heat inputs and process durations. Despite these variations in duration, upset, and power input, the weld strengths and elongations showed minor variations in performance. The pictures of an example set of welds are displayed in Fig. 11.

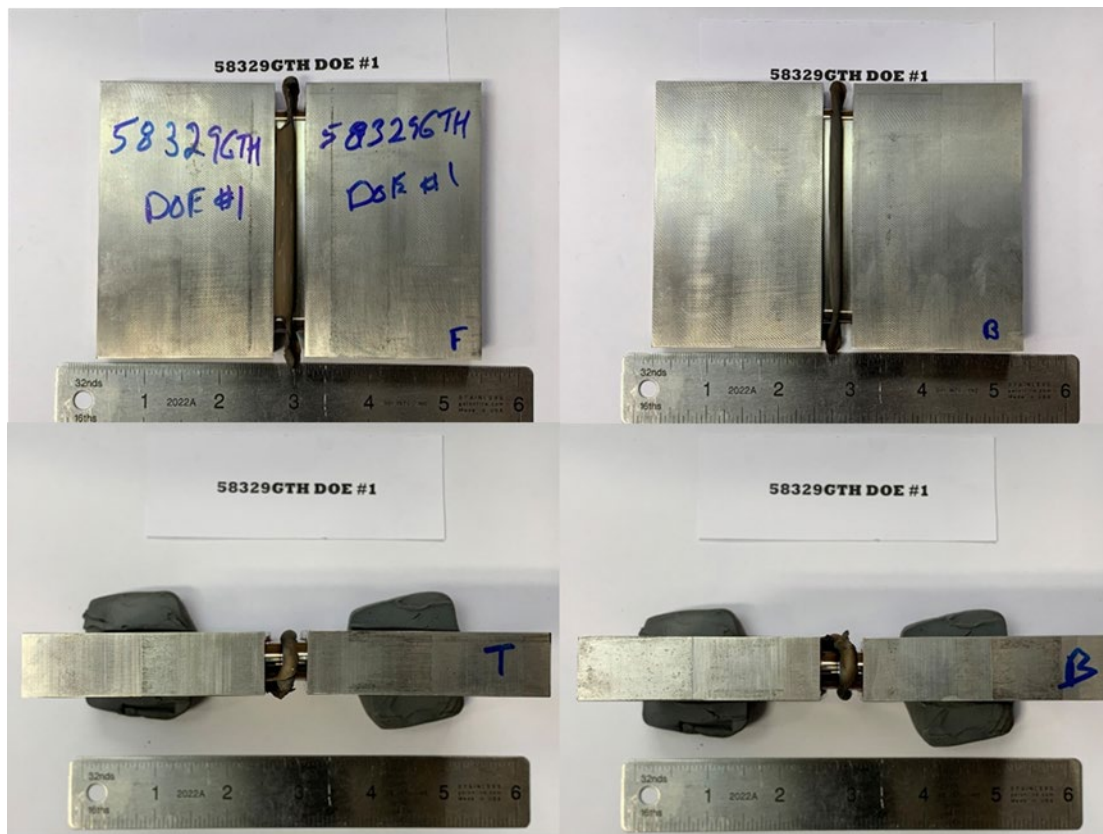


Fig. 11 Front, back, top and bottom view of LFW Ti-6Al-4V workpieces.

Table 8 LFW results for mechanical testing and process outputs.

Run Order	Weld Stage Duration (s)	Upset (mm)	Weld Yield Strength (MPa)	Ultimate Tensile Strength (MPa)	Elongation (%)
1	1.71	2.42	950 - 970	1010 - 1040	4 - 7
2	0.9	5.04	950 - 970	1010 - 1040	4 - 7
3-4	0.9 - 1.8	2.5 – 5.5	980 - 1000	1050 - 1080	4 - 7
5-12	0.7 – 2.7	2.2 – 5.2	950 - 970	1020 - 1050	4 - 7

The largest factor for weld duration is surface velocity. As surface velocity increases, heat input is greatly increased. The more heat is applied, the quicker upset occurred and the shorter the weld duration became. Burn-off had the next largest influence, and is somewhat self-explanatory as the more burn-off that is required, the longer the weld duration. The pressure also had a significant influence on weld duration. As upset occurs when yielding occurs, increasing the pressure lower the required heating to produce upset.

G. Verification and Validation of LFW Model

The developed SPH model was run with the same boundary conditions as the experimental welding trials, with weld pressure of 140 MPa, frequency of 50 Hz, and amplitude of 2.5 mm. As a result, the weld duration and upset of each trial can be validated with experimental results in Table 8. Fig. 12 shows the temperature profile of LFW trial #2 of Ti-6Al-4V to Ti-6Al-4V. Initially, the two workpieces were 1 mm apart, and at room temperature of 300 K. The left workpiece was under pressure in x-direction, and the right workpiece oscillated in y-direction. At time $t = 0.1$ s, the temperature at the PZ started to increase due to frictional contact. Fig. 13 shows the temperature profile at 0.7 s and 0.745 s. At time 0.745 second, the upset was 5 mm.

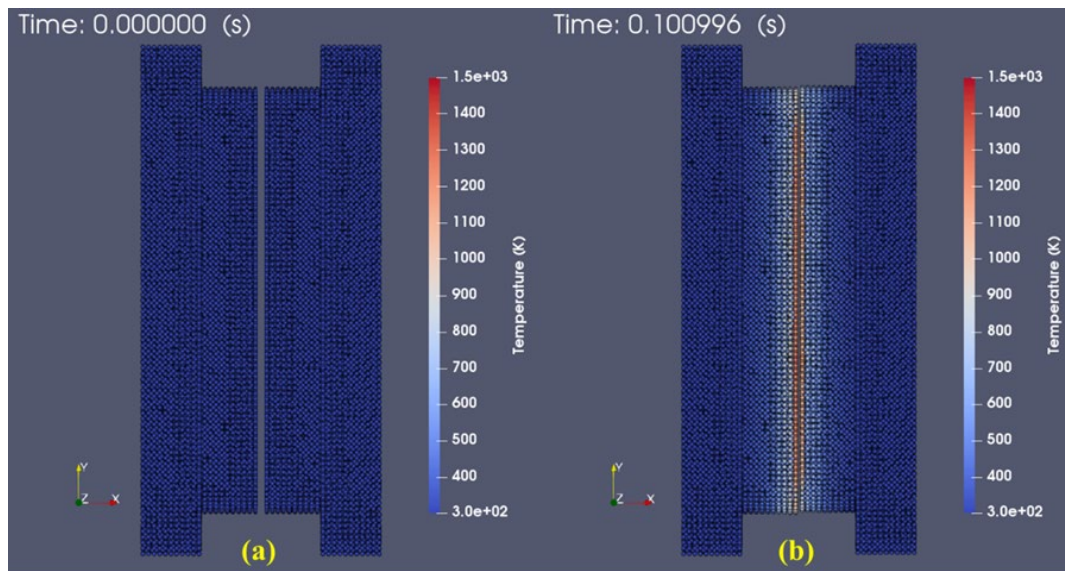


Fig. 12 LFW of Trial #2 (Ti-6Al-4V to Ti-6Al-4V) temperature profile at time (a) $t = 0$ s, and (b) $t = 0.1$ s. Initial positions of the workpieces were 1 mm apart. At $t = 0.1$ s, temperature at the PZ increased due to frictional contact.

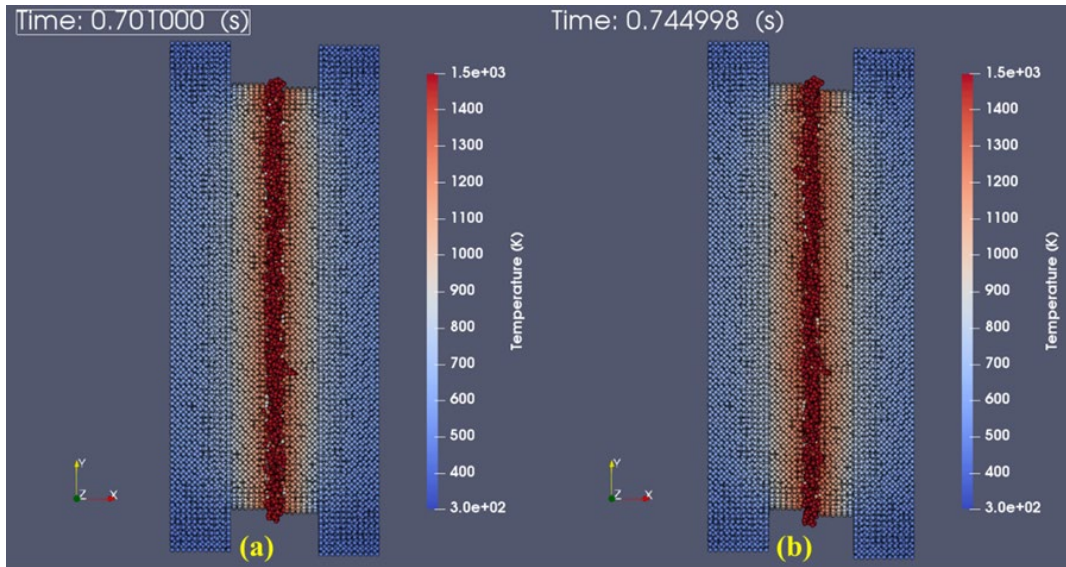


Fig. 13 LFW of Trial #2 (Ti-6Al-4V to Ti-6Al-4V) temperature profile at time (a) $t = 0.7$ s, and (b) $t = 0.745$ s. The upset at 0.745 s was 5 mm, agreed well with experimental upset.

As a result, the simulation upset was 5 mm and matched with the upset from experimental welding trials. However, the weld time of simulation (0.745 second) did not match with experiment (0.9 second). In this model, we did not account for surrounding factors such as convection and oxidation. The difference in welding time between simulation and experiment might come from those surrounding factors.

V. Conclusion

An SPH framework was developed capable of modeling of LFW process in 3D. The frictional heat generation term and modified material properties of Ti-6Al-4V were implemented into LS-DYNA as user defined function, enabling full 3D modeling of LFW process. Coulomb friction law is only applied at early stage of welding when interface temperature is low. As the interface material is plasticized, heat generation is dependent on plastic deformation. The LFW process of two distinct Ti-6Al-4V workpieces were simulated in LS-DYNA, and showed realistic flash formation. The SPH model demonstrated computational efficiency of approximately 16 hours to simulate 3 seconds of LFW process with a 12-core desktop workstation.

Parametric sensitivity study on influence of particle's interaction parameter (*PFACT* in LS-DYNA) and material properties on LFW flash formation was performed. Based on the sensitivity analysis of the model to *PFACT*, we identified that a *PFACT* value of 10^5 to be suitable for LFW conditions. A sensitivity study on influence of material properties on LFW flash formation was also undertaken. The varying values were the Young's modulus and yield stress of Ti-6Al-4V at high temperature above 1300K. As a result, lower values of Young's modulus and yield stress caused the flash to be thinner, weaker, and potentially disconnected from the weld.

Experimental welding trials of Ti-6Al-4V workpieces were performed to validate the model. Despite variation in weld duration, upset, and power input, the weld strengths and elongations showed minor variations in performance. Based on the weld trials results, the largest factor for weld duration is surface velocity. Temperature is greatly increased as surface velocity increases. Burn-off had the next largest influence, especially on weld duration. Pressure also had a significant influence on weld duration, due to the rise in heat input when increasing pressure.

The SPH model was validated with welding trial's results, using the same operating conditions. In this comparative study, the simulated flash was realistic and the upset from the simulation (of 5 mm) matched with the upset from the experiment. However, the simulation's weld time (0.745 second) did not match with the trial's (0.9 second). In summary, SPH based methods provide new capabilities for process modeling of LFW which could offer new tools for investigating LFW virtually. However, further research is needed to improve fidelity of the simulation framework for blind predictions and to mature the models into standalone tools.

Acknowledgments

The research presented here was funded by an Air Force SBIR/STTR Phase II program, contract FA8650-19-C-5050, under Topic: AF181-051, awarded to Advanced Cooling Technologies, Inc. (ACT). The principal investigator

for the program was Dr. Srujan Rokkam. Mr. Quang Truong was the project engineer. The experimental work was undertaken at Edison Welding Institute, by Dr. Michael Eff. The authors would like to thank the technical monitors from AFRL Wright- Patterson AFB, OH for their support and technical discussions. Paper approved for public release per AFRL-2023-0066.

References

- [1] Maalekian, "Friction welding - critical assessment of literature," *Science and Technology of Welding and Joining*, Vol 12, No 8, 708-729, 2007.
- [2] Bhamji I, Preuss M, Threadgill PL, Addison AC., "Solid state joining of metals by linear friction welding: a literature review," *Mater Sci Tech*, 27: 2-12, 2011.
- [3] Gianluca Buffa, et al., "Experimental and numerical analysis of microstructure evolution during Linear Friction Welding of Ti-6Al-4V titanium alloys," *Procedia Manufacturing*, Vol. 1, Pages 429-441, 2015.
- [4] Wenya Li, et al., "Numerical Simulation of Friction Welding Processes Based on ABAQUS Environment," *Journal of Engineering Science and Technology Review* 5 (3) 10-19, Special Issue on Simulation of Manufacturing Technologies, 2012.
- [5] Mica Grujicic, et al., "Process Modeling of Ti-6Al-4V Linear Friction Welding (LFW)," *Journal of Materials Engineering and Performance*, Vol. 21(10), October 2012.
- [6] www.taylor-winfied.com/linear-friction-welding/
- [7] Wenya Li, Feifan Wang, Shanxiang Shi, and Tiejun Ma, "Numerical Simulation of Linear Friction Welding Based on ABAQUS Environment: Challenges and Perspectives," *Journal of Materials Engineering and Performance*, Volume 23(2), February 2014.
- [8] G. Buffa, et al., "Experimental and numerical analysis of microstructure evolution during Linear Friction Welding of Ti6Al4V titanium alloys," *Procedia Manufacturing*, Vol. 1, Pages 429-441, 2015.
- [9] Carmine Capone, "Numerical Simulation of Fluid-Structure Interaction comparing SPH and ALE Approaches," University of Naples "Federico II", Naples, Italy, 80125, 2010.
- [10] Bhojwani S., "Smoothed Particle Hydrodynamics modelling of the friction stir welding process," Ann Arbor, MI, ProQuest, 2007.
- [11] Tartakovsky AM, et al., "Modeling of friction stir welding process with smooth particle hydrodynamics," SAE International, 2006.
- [12] Limido J, et al., "SPH method applied to high-speed cutting modelling," *International Journal of Mechanical Sciences*, 49:898-908, 2007.
- [13] Xu, J.; Wang, J., "Interaction methods for the SPH parts (multiphase flows, solid bodies) in LS-DYNA," Proceedings of the 13th International LS-DYNA Users Conference, Detroit, MI, USA, June 2014.